Article

SPECTROSCOPIC PROPERTIES OF Fe^{2+} DOPED $Zn_3(PO_4)_2$ ZnO NANOCRYSTALLINE POWDER

Sandhya Cole*

Department of Physics, Acharya Nagarjuna University, Nagarjuna Nagar, Guntur - 522 510, India

Citation: Sandhya Cole

Specttroscopic properties of Fe2+ doped Zn3(PO4)2 ZnO nanocrystalline powder

J.Adv.Sci.Eng&Tech, 4,1,2024, 20

Received on
12th Novemeber 2024

Revised on
19th January 2024

Accepted on
25th January 2024

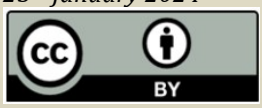

Abstract

Among all the phosphates, Zinc phosphate has wide spread applications in coating, electric motors, transformers, and the automotive industry. It is also widely used as an alternative to several non toxic and anticorrosive pigments. Fe^{2+}doped $Zn_3(PO_4)_2$ZnO nanopowders are prepared at room temperature using ball milling technique. The spectral and structural characterizations are X-ray diffraction and SEM. The average crystallite sizes of prepared nanopowders are calculated from the XRD data and are around 50 to 60 nm and the crystal unit cell of the nanoparticles is found to have monoclinic structure. The morphology of the nanoparticles is studied using scanning electron microscopy. The present investigation focused on the phase evolution of Fe^{2+}doped $Zn_3(PO_4)_2$ZnO nanopowders by high-energy ball milling technique.

Keywords: Iron ions, Ball milling, XRD, Optical absorption, SEM.

1. Introduction

Nanocrystalline materials [1] are defined as materials with grain sizes less than 100 nm received much attention as advanced engineering materials with improving physical and mechanical properties [2]. High-energy ball milling (HEBM) is known to induce chemical reactions in powder mixtures, a process usually termed mechanochemistry. During the last decade, HEBM has proved to be an exciting technique for the transformation of known materials and the synthesis of new ones. A broad range of ceramics and cermets composites, amorphous and nanocrystalline alloys as well as high temperature phases of nitrides, carbides and silicides have been produced by applying the HEBM technique with different experimental setups [3-5]. Self-sustained combustion can also occur for exothermic mixtures of reactants, provided the transferred mechanical energy is enough to put the starting powders to a critical metastable state [6]. For lower energy ranges, this technique has been applied to solid/liquid mixtures as a tool for making homogeneous dispersion at industrial scales, such as paint and coating pro-

duction techniques [7, 8]. However, a limitation for this approach is related to the chemical reactions that yield nondesire surface phases or even dissolution of the solid phase onto the liquid carrier.

Zinc phosphate ($Zn_3(PO_4)_2$) is the most significant multifunctional material for potential applications, like eco-friendly anticorrosive pigments and dental cements due to its low solubility in water and biocompatibility [9, 10]. $Zn_3(PO_4)_2$ is also one of the best luminescent material, widely used in fluorescent lamps, light emitting displays, cathode-ray tubes and white light emitting diodes (LEDs) [11-13]. The research on zinc oxide (ZnO) nanopowders has paid an attention to large extent due to their versatile properties - near UV [14], visible emission [15-17], optical transparency [18], electrical conductivity [19] and many other potential applications in transducers, gas sensors, transparent conducting coating materials, optical solar cells [20] etc. Nanomaterials are useful in daily life various applications in the field of medicine, solar cells, water purification, pharmaceutical and catalysts etc [21]. The design of nanostructure materials with different shapes has given an impetus to the development of nanoscience and nanotechnology [22-24].

Among the oxides of transition metal, zinc oxide (ZnO) is considered to be one of the most important multifunctional semiconductor material for technological applications such as light emitting diodes, gas sensors, drug delivery, transparent field effect transistors, window layer for thin-film solar cells, transparent conducting electrodes, surface acoustic wave devices, piezoelectric devices, photodiodes and optoelectronic devices due to the wide band gap (3.37 eV), high transmission coefficient in the visible and near infrared spectral range and large excitation binding energy (60 meV) at room temperature [25, 26].

The present work reports the effect of doping on the structural and morphology and phase purity of $Zn_3(PO_4)_2$ZnO nanocrystalline powder synthesized by ball milling method at different doping concentrations of Fe ions. It is observed that the particle size of undoped and Fe ion doped $Zn_3(PO_4)_2$ZnO nanostructures increases while optical band gap decreases as we increase the doping concentration.

2. Experimental

2.1 Composite Preparation

The starting materials are analar grade chemicals of zinc phosphate ($Zn_3(PO_4)_2$), zinc oxide (ZnO) and Iron-oxide (Fe_2O_3) with 99.9% purity. Synthesis of zinc phosphate-based composite nanopowders consists of mechanical activation of powder mixture. The obtained mixture is milled in a high energy planetary ball mill for 5h. Mechanical activation is carried out using zirconia balls (diameter 20 mm). The ball to powder weight ratio and milling speed are 10:1 and 350 rpm respectively. The total powder mass is 10 gm. The $Zn_3(PO_4)_2$ZnO powder is taken and different concentrations of Fe_2O_3 (0.1%, 0.3% and 0.5%) are doped and repeated with the ball milling

process. Details of process specifications and abbreviated name of powders are given in Table 1.

S. No	Composition	Name of the Powder
1	100 wt % $Zn_3(PO_4)_2ZnO$	(F_0) Undoped
2	99.9 wt % $Zn_3(PO_4)_2ZnO$ + 0.1% Fe_2O_3	(F_1) 0.1% doped Fe_2O_3
3	99.7 wt % $Zn_3(PO_4)_2ZnO$ + 0.3% Fe_2O_3	(F_2) 0.3% doped Fe_2O_3
4	99.5 wt % $Zn_3(PO_4)_2ZnO$ + 0.5% Fe_2O_3	(F_3) 0.5% doped Fe_2O_3

Table 1: Specifications of the synthesis process and abbreviated names of Powders

2.2 Characterization techniques

The XRD powder diffraction pattern of prepared undoped and Fe_2O_3 doped $Zn_3(PO_4)_2ZnO$ nanopowders are recorded using on XRD-6100 SHIMADZU X-Ray diffractometer in the scanning range of 10-80^0 (2θ) using Cu K_α radiation having a wavelength of 1.5406Å at room temperature. The optical UV-Visible absorption spectra of prepared nanopowders are recorded using JASCO V-670 UV-VIS-Spectrophotometer in the wavelength region 200-1200 nm. The surface morphology and phase purity are studied by scanning electron microscopy (ZEISS) with an accelerating voltage of 20 KV.

3. Results and discussion

X-ray diffraction

The sample is scanned for 2θ in the range 10-80° at a scan rate of 1°/min and the obtained diffraction pattern is shown in Fig.1. Sharp peak intensities in the X-ray diffraction spectra indicate high crystalline nature. The XRD pattern of the zinc phosphate nanocrystalline powder exhibits the strong peaks for 2θ values at 19.30°, 21.10°, 24.60°, 28.33°, 29.24°, 31.75°, 34.41°,36.24°, 37.48°, 39.16°, 40.52°, 42.60°, 43.36°, 46.61°, 47.54°, 49.02°, 49.64°, 51.04°, 56.59°, 59.56°, 61.62°, 62.86°, 69.07° which are indexed to the (011), (111), ($\bar{3}$11), (202), ($\bar{4}$11), (600), (022), (420), (213), ($\bar{4}$22),

($\bar{6}$13), (602), ($\bar{8}$02), (711), ($\bar{8}$04), (802), (115) planes are indexed to monoclinic structure of zinc phosphate ($Zn_3(PO_4)_2$) which are matched with the standard XRD data of JCPDS file (Number: 29-1390) and (100), (002), (101), (102), (110), (201) planes respectively are indexed to hexagonal wurtzite structure of ZnO JCPDS file (Number: 36-1451).. The mean crystallite size (D) can be evaluated from the full width at half maximum (FWHM) of the diffraction peaks. According to Debye - Scherrer's equation [27].

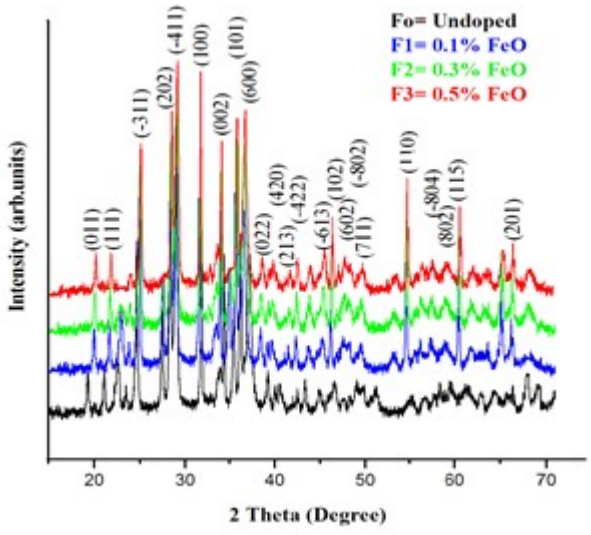

Fig. 1: XRD pattern for undoped and Fe_2O_3 doped $Zn_3(PO_4)_2$ZnO nanopowders

$$D = \frac{0.89\lambda}{\beta cos\theta} \quad (1)$$

The lattice strain (ε) is also calculated for the same diffraction lines from the following equation.

$$\varepsilon = \frac{\beta}{4\tan\theta} \quad (2)$$

Here, D is the mean grain size, λ is the X-ray wavelength, β is the full width of half maximum (FWHM) intensity of diffraction line and θ is the diffraction angle and ε is the lattice strain. The grain size and lattice strain of the samples are calculated from equations (1) and (2) using reflection in the XRD pattern. Different dopant concentrations are added and the calculated values of particle size and lattice strain-are given in Table 2. The lattice cell parameters and unit cell volume of undoped and different concentrations of Fe_2O_3 doped $Zn_3(PO_4)_2$ZnO nanopowders are calculated and furnished in Table 3. The average crystallite size is calculated from the most intense diffraction peak at 54-60 nm.

S. No	sample	Diffraction angle (2θ)	Grain Size nm
1	F_0	29.40	59.11
2	F_1	29.50	55.59
3	F_2	29.65	55.55
4	F_3	29.80	54.11

Table 2: Particle size variations of un doped and Fe_2O_3 doped $Zn_3(PO_4)_2$ZnO nano powders from XRD pattern

Sample	$Zn_3(PO_4)_2$ Lattice Parameters			Unit Cell Volume (V)
	a	b	c	
F_0	16.18	4.85	8.49	643.81
F_1	14.97	5.63	8.19	667.93
F_2	14.99	5.64	8.19	669.28
F_3	14.97	5.64	8.20	668.77
Ref. JCPDS: Card No. 29-1390	15.00	5.63	8.18	668.37

Sample	ZnO Lattice Parameters		Unit Cell Volume (V)
	a(=b)	c	
F_0	3.24	5.20	47.42
F_1	3.25	5.20	47.67
F_2	3.24	5.20	47.60
F_3	3.25	5.20	47.64
Ref. JCPDS: Card No. 36-1451	3.24	5.20	47.62

Table 3: 3a & 3b Lattice parameters and unit cell volume variations of un doped and Fe_2O_3 doped $Zn_3(PO_4)_2$ZnO nano powders from XRD pattern

SEM and EDX analysis

Fig.2 shows the typical SEM micrograph of the undoped and Fe^{2+} doped $Zn_3(PO_4)_2ZnO$ nanopowders with their corresponding energy dispersive X-ray (EDX) spectroscopy results. It is observed that the undoped and Fe^{2+} doped $Zn_3(PO_4)_2ZnO$ powders are well separated and defined in the grain size range of 50-60 nm. In this method, the increase in the particle size is due to the growth of fine nanoparticles together by solid state diffusion and thereby reducing the surface area of the nanoparticles to have a better crystalline and homogeneity. The calculated crystallite size of the samples matches well with the XRD pattern of single phase monoclinic structure of $Zn_3(PO_4)_2$. EDX spectroscopy confirms that the samples consist primarily of Zn, P and O and matches well with their starting amounts.

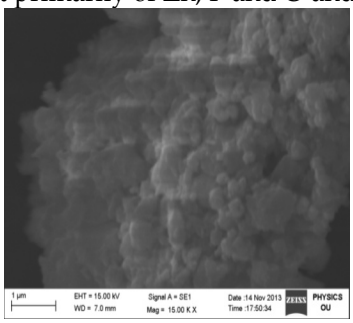

Undoped $Zn_3(PO_4)_2ZnO$

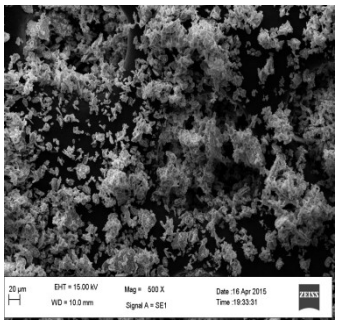

0.1% Fe_2O_3 doped $Zn_3(PO_4)_2ZnO$

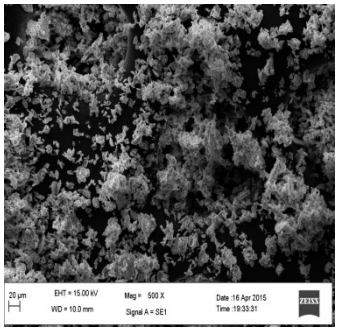

0.3% Fe_2O_3 doped $Zn_3(PO_4)_2ZnO$

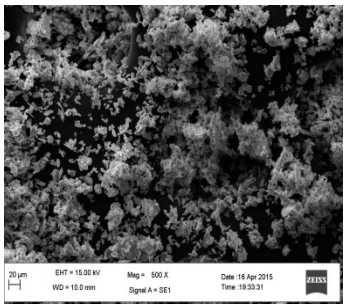

0.5% Fe_2O_3doped $Zn_3(PO_4)_2ZnO$

Fig. 2: SEM Images for Undoped and Fe_2O_3 doped $Zn_3(PO_4)_2ZnO$ nanopowders

Conclusion

Undoped and Fe_2O_3 doped $Zn_3(PO_4)_2ZnO$ nanopowders are prepared by the ball milling technique. X-ray analysis of undoped and Fe_2O_3 doped nanopowders reveal that powder belongs to monoclinic system, crystallite size and lattice cell parameters and unit cell volume are evaluated, which are in good agreement with the reported values. SEM image gives the formation of non uniform particles and a notable tendency of crystalline growth and agglomeration. From EDS spectral analysis, it is confirmed that the observed atomic percentages of Zn, P, O and Fe matched well with their starting amounts.

References

[01] H. Gleiter, Prog. Mat. Sci. 33 (1990) 4.

[02] H. Hahan, NanoStructured Mat. 9 (1997) 3.

[03] Y. Zhao, J. Qian, L.L. Daemen, C. Pantea, J. Zhang, G.A. Voronin, T.W. Zerda, Appl. Phys. Lett. 84 (2004) 1356.

[04] W.A. Kaczmarek, S.J. Campbell, Mater. Sci. Forums 269 (1998) 259.

[05] L. Takacs, Appl. Phys. Lett. 69 (1996) 436.

[06] L. Takacs, Mater. Sci. Forum 269 (1998) 513.

[07] P.K. Panigrahy, G. Goswami, J.D. Panda, R.K. Panda, Cement Concrete Res. 33 (2003) 945.

[08] I.A. Susorov, Russ. J. Appl. Chem. 71 (1998) 1825.

[09] Del Amo, B. Romagnoli, R. Vetere, V.F. Hernandez, L.S. Prog. Org. Coat. 33 (1998) 28.

[10] D.C. Look, Mater. Sci. Eng. B 80 (2001) 383.

[11] Li Li, Cao Xue-q in, Zhang You, Guo Chang-xin. Trans. Nonferrous Met. Soc. China 22 (2012) 373.

[12] M. Ferhi, K. Horchani-Naifer, M. Ferid, J. Lumin. 128 (2008) 1777.

[13] Gao Rui, Qian Dong, Li Wei. Trans. Nonferrous Met. Soc. China 20 (2010) 432.

[14] Eva M. Wong, Peter C. Searson, Appl. Phys. Lett. 74 (1999) 2939.

[15] K. Vanheusden, C.H. Seager, W.L. Warren, D.R. Tallant, J.A. Voigt, Appl. Phys. Lett. 68 (1996) 403.

[16] H.Q.Wang, G.Z. Wang, L.C. Jia, C.J. Tang and G.H. Li, J. Phys. D: Appl. Phys. 40 (2007) 6549.

[17] Q.P Wang, D.H. Zhang, Z.Y. Xue, X.T. Hao, Applied Surface Science. 201 (2002) 123.

[18] Ma Jina, Ji Fenga, Zhang De-hengb, Ma Hong-leia, Li Shu-ying, Thin Solid Films. 357 (1999) 98.

[19] Jason B. Baxter, Charles A. Schmuttenmaer, J. Phys. Chem. B. 110 (2006) 25229.

[20] Yasuhide Nakamura-Materials, Nnin Reu, Research Accomplishments (2006) 74.

[21] R. Manimaran, K. Palaniradja, N. Alagumurthi, S. Sendhilnathan, J. Hussain, Appl. Nanosci. (2013)1.

[22] Alivisatos, A. P. Science 271 (1996) 933.

[23] Y. Xia, P. Yang, Y. Sun, Y. Wu, B. Mayers, B. Gates, Y. Yin, F. Kim, H. Yan, Adv. Mater. 5 (2003) 353.

[24] J. Zhang, L. Sun, J. Yin, H. Su, C. Liao, C. Yan, Chem. Mater. 14 (2002) 4172.

[25] J. Geng, D. Lu, J. Zhu, H. Chen, J. Phys. Chem. B 110 (2006) 13777.

[26] L. Qian, Z. Liu, Y. Mo, H. Yuan, D. Xiao, Mater. Lett., 100 (2013) 124.

[27] Z. L. Wang, ACS Nano, 2 (2008) 1987.

[28] C.S. Tiwary, R. Sarkar, P. Kumbhar, A.K. Mitra, Phys. Lett. A 372 (2008) 5825.